Manuscript prepared for Atmos. Chem. Phys.
with version 2014/09/16 7.15 Copernicus papers of the LaTeX class copernicus.cls.
Date: 29 May 2015

Investigation of the adiabatic assumption for estimating cloud micro- and macrophysical properties from satellite and ground

D. Merk[1], H. Deneke[1], B. Pospichal[2], and P. Seifert[1]

[1]Leibniz Institute for Tropospheric Research, Leipzig, Germany
[2]Leipzig Institute for Meteorology, Leipzig, Germany

Correspondence to: D. Merk (merk@tropos.de)

Abstract. In this study the accuracy of quantities relevant for diagnosing the first indirect aerosol effect with satellite is investigated by comparing co-located ground-based and spaceborne observations. The focus is set on retrievals of cloud droplet number concentration and cloud geometrical depth. For the study we considered the sub-adiabatic cloud model which is commonly applied to retrieve cloud micro- and macrophysical quantities from passive satellite sensors like SEVIRI or MODIS. As reference we use ground-based observations from a cloud radar, a microwave radiometer and a ceilometer from which cloud droplet number concentration is derived with a newly developed optimal estimation technique. Although the ground-based observations contain detailed information about the cloud vertical structure, large uncertainties in the retrieved cloud microphysical properties were found. We investigate four different cases (27 October 2011, 1 June 2012, 27 September 2012 and 21 April 2013) of temporally homogeneous and inhomogeneous liquid cloud layers observed over Germany. Considering uncertainties for both ground-based and satellite-based retrievals, we find a good agreement when temporally homogeneous single-layer clouds are considered. Overall, cloud layers were sub-adiabatic with medians of the adiabatic factor around 0.65 for 3 cases and around 0.45 for one case. When satellite-based and ground-based retrievals are compared, the best agreement was found for the 21 April 2013 homogeneous case, namely a 4 % relative mean difference of cloud geometrical depth and a 15 % relative mean difference of cloud droplet number concentration when the sub-adiabatic factor obtained from ground-based observations is considered. For all evaluated cases, the current SEVIRI retrieval seems to underestimate the effective radius relative to ground-based and MODIS measurements for unfavourable solar zenith angles of above approximately 60°. This deviation strongly propagates to the derived cloud droplet number concentration.

1 Introduction

Low-level liquid clouds play an important role in the energy balance of the Earth, and are found in many areas around the globe. Their microphysical and optical properties are strongly influenced by aerosol particles that act as cloud condensation nuclei (CCN). Twomey (1974) first postulated the effect of an increased aerosol number concentration in clouds, which is commonly referred to as the first indirect aerosol effect, as a climatically relevant process. The quantification of such aerosol indirect effects remains one of the main uncertainties in climate projections (Boucher et al., 2013). If the liquid water content as well as the geometrical depth of the cloud are considered constant, a higher aerosol load results in an enhanced cloud albedo. This effect is observed in particular by means of ship tracks that form in marine stratocumulus cloud decks (e.g. Ackerman et al., 2000). The chain of interactions of cloud microphysics and dynamics is complex and not yet fully understood. However, to quantify the effect of a change in the aerosol load on cloud albedo, it is necessary to consider both microphysics and macrophysics, which are influenced by cloud dynamical processes. Brenguier et al. (2000) noted that a 15 % change in the cloud geometrical depth (H_{cloud}) can have a similar effect on cloud albedo as a doubling of the cloud droplet number concentration (N_{d}). Already Han et al. (1998) suggested to investigate a column cloud droplet number concentration which combines H_{cloud} and N_{d}. These two quantities turned out to be the key parameters for quantifying the aerosol effect on cloud albedo.

The aim of the current study is to gain a better understanding of the current possibilities and shortcomings when H_{cloud} and N_{d} of clouds are retrieved from satellite observations, by evaluating existing retrievals with ground-based observations performed over Germany. We combine observations from SEVIRI (Spinning Enhanced Visible and InfraRed Imager) onboard Meteosat Second Generation (MSG) and MODIS (Moderate-Resolution Imaging Spectroradiometer) onboard Terra and Aqua with ground-based remote sensing data obtained with ceilometer, microwave radiometer and 35-GHz cloud radar at Leipzig, Germany (51.35 N, 12.43 E) and at Krauthausen, Germany (50.897 N, 6.46 E). Those ground-based instruments are operated in the framework of Cloudnet (Illingworth et al., 2007) and ACTRIS (Aerosols, Clouds and Trace gases Research InfraStructure Network).

The combination of ground-based ceilometer and cloud radar is able to provide reliable detection of cloud geometric borders (Boers et al., 2000; Shupe, 2007; Illingworth et al., 2007; Martucci et al., 2010). To derive N_{d} with this set of ground-based instruments Rémillard et al. (2013) recently suggested a radar-radiometer retrieval based on a condensational growth model taking the vertical velocity into account and allowing small variations of N_{d} with height, while it is assumed vertically constant in most other studies. Since Cloudnet does not provide N_{d}, we developed and apply an optimal estimation technique to obtain N_{d}, based on the method introduced by Fox and Illingworth (1997), similarly also applied in Rémillard et al. (2013). Given other instrument combinations such as those including lidar measurements (Schmidt et al., 2014a), (Martucci and O'Dowd, 2011) or solar radiation measurements (Dong et al., 1997, 2002) would give alternative opportunities to derive N_{d}. Due to the under-constrained nature and assumptions made in such retrieval methods, substantial differences for the obtained microphysical parameters may occur, as pointed out by Turner et al. (2007), who intercompared several ground-based retrieval methods for one case study.

While remote sensing observations from ground are always column measurements, passive satellite observations from, e.g., SEVIRI or MODIS, show a good spatio-temporal coverage and are therefore suitable to investigate the first indirect aerosol effect on a larger scale. Active satellite sensors on the other hand, such as the cloud profiling radar onboard CloudSat (Stephens et al., 2002) or the Cloud-Aerosol-Lidar with Orthogonal Polarization (CALIOP) onboard CALIPSO (Winker et al., 2009, Cloud-Aerosol Lidar and Infrared Pathfinder Satellite Observation), are able to provide vertically resolved cloud observations over larger areas that can be used to investigate aerosol effects on cloud properties (e.g. Christensen and Stephens, 2011), but lack highly-resolved temporal coverage and have a smaller scanning swath than passive sensors onboard polar-orbiting satellites.

Despite their coarser spatial resolution, geostationary satellite observations benefit from the high temporal coverage of up to 5 minutes in conjunction with a high spatial coverage. This can be considered as an advantage for the determination of large-scale first indirect aerosol effects. Within this study the capabilities of geostationary satellites for cloud retrievals will be further evaluated. Validation of satellite-derived cloud parameters, such as (Q_{L}), with ground-based observations has only infrequently been performed Roebeling et al. (2008b, a); Hünerbein et al. (2014). Especially the comparison of N_{d} and H_{cloud} from both space and ground has not yet been carried out intensively for different regions of the Earth, although Placidi et al. (2007) pointed out that their combined retrieval of N_{d} and H_{cloud} would give the opportunity to derive the first indirect effect with high spatial and temporal resolution. In this study, we contrast satellite retrievals with the independently retrieved properties from ground-based remote sensing. To our knowledge such evaluations from the SEVIRI instrument for the indirect aerosol effects' key parameters have been rarely carried out (e.g. in Roebeling et al. (2008a)). Previous satellite retrieval studies, retrieving N_{d} and/or H_{cloud}, usually apply a (sub-)adiabatic cloud model with a presumed adiabatic factor (e.g. Schueller et al., 2003; Boers et al., 2006; Bennartz, 2007). Only Min et al. (2012) calculated this factor in advance. With that, we can assess the influence of cloud sub-adiabaticity on N_{d} and H_{cloud} as well as the agreement between the retrieved properties from ground and satellite. Apart from assumptions about the adiabatic factor, also uncertainties in the retrieval of optical depth and effective radius determine the accuracies of the results and will be discussed in this context.

The paper is structured as follows. In Sect. 2 we introduce the adiabatic model, relevant for the satellite-based retrieval of key parameters, as well as the retrieval methods from ground. Afterwards we describe the instruments and data processing tools used within this study in Sect. 3. In Sect. 4 these retrievals are applied to four different cases which are then used to evaluate the satellite-based observations. Finally, a conclusion and outlook is given in Sect. 5.

2 Cloud microphysical retrieval methods

In this section we present the theory of the (sub-)adiabatic cloud model and retrieval strategies for the cloud droplet number concentration from the suite of ground-based instruments.

2.1 Retrievals using the (sub-)adiabatic cloud model

For a moist rising air parcel liquid water content $q_{\mathrm{L}}(z)$ increases linearly with height (Albrecht et al., 1990) and can be related to $N_{\mathrm{d}}(z)$ and the mean volume droplet radius $r_{\mathrm{v}}(z)$:

$$q_L(z) = f_{\mathrm{ad}}\Gamma_{\mathrm{ad}}(T,p)z = \frac{4}{3}\pi\rho_{\mathrm{w}}r_{\mathrm{v}}^3(z)N_{\mathrm{d}}(z) \tag{1}$$

Here z is the height above cloud base, ρ_{w} is the density of water. f_{ad} represents the sub-adiabatic fraction of liquid water content, in the following simply called adiabatic factor. It can be explained by the reduction of liquid water due to evaporation influenced by the entrainment of drier air masses and leads to $f_{\mathrm{ad}} < 1$ (sub-adiabatic). $\Gamma_{\mathrm{ad}} = A_{\mathrm{ad}}(T,p)\rho_{\mathrm{a}}(T,p)$ is the adiabatic rate of increase of liquid water content, with ρ_{a} the air density and A_{ad} the adiabatic increase of the liquid water content mixing ratio. In general, for the adiabatic factor f_{ad} a range of $[0.3, 0.9]$ is seen as common (Boers et al., 2006). From eq. (1) it is clear that either $N(z)$ or $r_{\mathrm{v}}(z)$ can be affected by evaporation. Boers et al. (2006) considers two extremes: (a) homogeneous mixing, where $N_{\mathrm{d}}(z)$ stays constant in the vertical layer, but the droplet radius ($r_{\mathrm{v}}(z)$) is changed due to evaporation, (b) inhomogeneous mixing, where the number of droplets change (dilution of whole droplets), but the droplet radius profile is unchanged. In nature, a mixture of both processes may likely occur (Lehmann et al., 2009). For our study we only consider homogeneous mixing.

In remote sensing usually the effective radius is retrieved. It is defined as the third over the second moment of the droplet size distribution (Hansen and Travis, 1974) and can be linked to the mean volume radius (r_{v}) with the following relationship:

$$r_{\mathrm{e}}^3 = k^{-1} r_{\mathrm{v}}^3 \qquad (2)$$

The factor k depends on the cloud type and corresponding typical droplet size distributions. Typical values for marine and continental liquid water clouds are 0.67 and 0.80, respectively (Brenguier et al., 2000).

This leads to the following two equations for optical depth τ and effective radius r_{e} (compare Eq. A12, A14 in Boers et al. (2006)):

$$\tau = \frac{6}{5}\pi^{1/3}\left(\frac{4}{3}\rho_{\mathrm{w}}\right)^{-2/3}(\Gamma_{\mathrm{ad}} f_{\mathrm{ad}})^{2/3}(kN_{\mathrm{d}})^{1/3} H^{5/3} \qquad (3)$$

and

$$r_{\mathrm{e}} = \left(\frac{4}{3}\pi\rho_{\mathrm{w}}\right)^{-1/3}(kN_{\mathrm{d}})^{-1/3}(\Gamma_{\mathrm{ad}} f_{\mathrm{ad}})^{1/3} H^{1/3} \qquad (4)$$

Without entrainment, we find $f_{\mathrm{ad}} = 1$ (adiabatic clouds) in all the equations above.

The typically obtained products from passive satellite remote sensing are τ and r_e using the Nakajima and King (1990) retrieval method. The (sub-)adiabatic cloud model can be used to derive cloud properties such as liquid water path (Q_{L}), cloud droplet number concentration (N_{d}) and geometrical depth (H) by inserting eq. 4 into eq. 3 and solving for the desired quantity.

$$N_{\mathrm{d}} = \frac{\sqrt{10}}{4\pi\rho_{\mathrm{w}}^{0.5} k}(f_{\mathrm{ad}}\Gamma_{\mathrm{ad}})^{0.5}\tau^{0.5} r_{\mathrm{e}}^{-2.5} \qquad (5)$$

$$H = \sqrt{\frac{10}{9}(f_{\mathrm{ad}}\Gamma_{\mathrm{ad}})^{-1}\rho_{\mathrm{w}}\tau r_{\mathrm{e}})} \qquad (6)$$

$$Q_{\mathrm{L}} = \frac{5}{9}\rho_{\mathrm{w}}\tau r_{\mathrm{e}} \qquad (7)$$

Various different values considered for k, Γ_{ad} and f_{ad} can be found in previous studies (Table 1) due to different climatic and geographical regions on Earth (e.g. continental vs. maritime). Often even adiabatic clouds are considered ($f_{\mathrm{ad}} = 1$) (e.g. Quaas et al., 2006). In this study we take a constant value for k ($k = 0.8$), and $\Gamma_{\mathrm{ad}}(T,p)$ using pressure and temperature obtained for cloud base height. The adiabatic factor is initially set to $f_{\mathrm{ad}} = 1$ for the satellite-derived values of N_{d} and H, but is also calculated from ground-based observations in a further step. Following Wood (2006) the adiabatic factor is given by the following relationship:

$$f_{\mathrm{ad}} = \frac{2Q_{\mathrm{L}}}{(H_{\mathrm{obs}}^{\mathrm{ground}})^2\Gamma_{\mathrm{ad}}(T,p)} \qquad (8)$$

We use Q_{L} from the ground-based microwave radiometer, $H_{\mathrm{obs}}^{\mathrm{ground}}$ as the difference of cloud top height from the cloud radar and cloud base height from the ceilometer, and $\Gamma_{\mathrm{ad}}(T_{\mathrm{cbh}}, p_{\mathrm{cbh}})$ using numerical weather prediction (NWP) data.

2.2 Ground-based retrieval of cloud droplet number concentration

2.2.1 Radar-radiometer based retrieval method

With the given observations, the retrieval of cloud droplet number concentration can be based on a combination of the cloud radar and the microwave radiometer. This mainly requires an assumption about the droplet size distribution. Cloud microphysical quantities can then be described in terms of moments of this droplet size distribution. The cloud droplet number concentration is equivalent to the zeroth moment, the mean radius to the first moment, the liquid water content is proportional to the third moment, while the effective radius is the third over the second moment, and the radar reflectivity factor is proportional to the sixth moment. Relating these moments gives the chance to fully describe a unimodal distribution following either a gamma or lognormal shape and therefore calculating other moments of the size distribution which are not directly observed (Rémillard et al., 2013). Following Fox and Illingworth (1997), we relate the measured radar reflectivity (Z) to q_{L} and N_{d}. Thereby it is assumed that the droplet size distribution can be described by a gamma distribution with parameter β, where β is the index of the gamma function following the size distribution definition in (Fox and Illingworth, 1997; Martucci and O'Dowd, 2011):

$$N(r) \propto Ar^{\beta} \exp(-Br) \tag{9}$$

Thereby B is the rate parameter and A a function of the rate parameter. A similar method has been applied in (Rémillard et al., 2013), but using a lognormal size distribution. Although N_{d} may vary vertically, it is commonly suspected that it stays nearly constant throughout the vertical column of a nonprecipitating cloud (Bennartz, 2007; Brenguier et al., 2000). To retrieve the column cloud droplet number concentration from the available single-layer observations, we integrate q_{L} over the cloud column and can therefore use Q_{L} from the microwave radiometer (compare Rémillard et al., 2013):

$$N_{\mathrm{d}}^{\mathrm{FI}} = \frac{9}{2\pi^2 k\rho^2} \frac{(\beta+6)!}{(\beta+3)!(\beta+3)^3} \frac{Q_L^2}{(\int \sqrt{Z} dz)^2} \tag{10}$$

Due to the relationship $N \propto \sqrt{(Z)}$, this retrieval method does not require the assumption of a linearly increasing liquid water content profile. Both, homogeneous and inhomogeneous mixing with dry air (Lehmann et al., 2009) can easily alter the microphysical quantities in clouds in ways not adequately adressed within such a retrieval scheme. For example, the size distribution may become skewed and not be accurately described with a gamma-shape anymore. However, Boers et al. (2006) and Janssen et al. (2011) found out, that both assumptions about the mixing process result in nearly the same vertically averaged N_{d}.

2.2.2 Optimal Estimation method

The Optimal Estimation (OE) method, presented in the following, aims on finding the most likely state given the observations, the a-priori and the error estimates. Therefore we try to minimize a cost function following Rodgers (2000). The OE retrieval of cloud droplet number concentration ($N_{\mathrm{d}}^{\mathrm{OE}}$) and the liquid water content profile is based on the radar-radiometer method.

We further assume a vertically constant N_{d}, a gamma-shaped droplet size distribution with parameter β. As before, q_{L}, N_{d}, and Z are nonlinearly related. We include error estimates for the observed quantities as well as an a-priori state together with its error estimate.

Our observation vector ($\boldsymbol{y}$) contains the radar reflectivity Z and the microwave radiometer Q_{L}. Our state vector ($\boldsymbol{x}$) contains the vertically-constant N_{d} and the natural logarithm of the vertical q_{L} profile. The logarithm is used to avoid the occurence of unphysical negative liquid water contents in the minimization process.

$$\boldsymbol{y} = (Z, Q_{\mathrm{L}})^T ; \boldsymbol{x} = (N_{\mathrm{d}}, \ln(q_{\mathrm{L}}))^T \tag{11}$$

The forward model ($F(\boldsymbol{x})$) for OE consists of two separate parts: a model (Eq. (12)) for the calculation of Q_{L}, and a model (Eq. (10)) for the calculation of N_{d} given the state vector $\boldsymbol{x}$.

$$Q_{\mathrm{L}} = \int \exp(\ln(q_{\mathrm{L}}(z)))\mathrm{d}z \tag{12}$$

The Jacobians are calculated numerically using finite differences for both methods as follows:

$$H(x) = \frac{\delta y_i}{\delta x_j} = \frac{F(x_i + dx_i) - F(x_i)}{dx_i} \tag{13}$$

We apply the Levenberg-Marquardt minimization method until convergence is reached (Hewison, 2007). Only profiles with all required input data are processed. Only 0.1 % of all the valid input profiles failed convergence within 30 iteration steps.

For the a-priori state vector, we assume that the liquid water profile follows the adiabatic scaled profile. For the a-priori N_{d} we set a value of $300\,\mathrm{cm}^{-3}$ which is a typical value for continental sites (Miles et al., 2000). We assume that there are no correlations between the elements in the covariance matrix, implying no correlations of the q_{L} uncertainties at different height levels and no correlations between q_{L} and N_{d} uncertainties. This is a rather simplistic assumption, but the variances are set reasonably large. The standard deviation for N_{d} is set to $300\,\mathrm{cm}^{-3}$ and for $\ln(\mathrm{q_L})$ to $2.5\ln(\mathrm{gm}^{-2})$.

Just as for the background error covariance matrix, we assume for the observation error covariance matrix that there is no cross-correlation, and that all off-diagonal terms are thus zero.

The observation error covariance can be split up into individual contributing parts such as forward model error, radiometric noise error, and representativeness error. In this study the representativeness error is neglected, since observations and state variables are on the same grid. Radiometric noise errors are given by the Cloudnet algorithm. The forward model error is estimated by applying values of β in the range of 1 to 6 to the radar forward model and taking the variance of the resulting reflectivity values for a sample cloud profile with a geometrical extent of 700 m and linearly increasing q_{L} in steps of $0.1\,\mathrm{gm}^{-2}$ per 100 m.

Given the retrieved $N_{\mathrm{d}}^{\mathrm{OE}}$ and the theoretical adiabatic liquid water content for the observed cloud geometrical depth, we are able to calculate an adiabatic radar profile applying the relationship of q_{L}, Z and N_{d} of Fox and Illingworth (1997). If we relate Z_{ad} to the Z_{obs} from the cloud radar we obtain a second method to calculate the adiabatic factor ($f_{\mathrm{ad}}^{\mathrm{OE}}$):

$$f_{\mathrm{ad}}^{\mathrm{OE}} = \frac{\int Z_{\mathrm{obs}} dz}{\int Z_{\mathrm{ad}} dz} \tag{14}$$

3 Data

3.1 Instruments and retrievals

Data from SEVIRI (Schmetz et al., 2002) are used for the geostationary satellite perspective. SEVIRI provides 12 spectral channels covering the visible, the near infrared, and the infrared spectrum. The channels used here have a nadir resolution of 3 km x 3 km. The spatial resolution decreases towards the poles and is about 4 km x 6 km over our region of interest (Central Europe). In this study we use the 5-min temporal resolution data from the Rapid Scan Service (RSS). The SEVIRI radiances in the different channels are used as input for the Nowcasting Satellite Application Facility (NWCSAF) algorithm (Derrien, 2012) which provides a cloud mask, cloud top height, and cloud classification.

The NWCSAF cloud mask is used for deriving cloud phase, cloud optical depth, and effective radius with the KNMI (Royal Netherlands Meteorological Institute) cloud physical properties (CPP) algorithm (Roebeling et al., 2006), developed in the context of the satellite application facility on climate monitoring (CMSAF, Schulz et al., 2009). To derive the cloud mask, different multispectral tests using SEVIRI channels are applied in order to discriminate cloudy from cloud-free pixels. The cloud top height for low, liquid clouds is obtained by using a best fit between measured brightness temperatures in the 10.8 μm channel and simulated values using the RTTOV radiative transfer model (Saunders et al., 1999) applied to atmospheric profiles from the ECMWF NWP model. Using a channel in the visible spectrum (0.6 μm) together with an absorbing channel in the near infrared (1.6 μm) (Nakajima and King, 1990), the CPP algorithm retrieves cloud optical depth as well as effective radius which are representative for the uppermost cloud part. As this method relies on solar channels it works only during daytime.

MODIS is an imaging spectrometer onboard the satellites Terra (descending node) and Aqua (ascending node) which probe the Earth's atmosphere from a polar orbit that results in one daytime overpass per satellite per day over the region of interest. MODIS measures in 36 bands in the visible, near-infrared, and infrared spectrum, with some bands having a spatial resolution of up to 250 m. The cloud physical properties (Platnick et al., 2003) are retrieved in a similar manner as for SEVIRI, but at 1 km spatial resolution using the channels 0.6 μm (band 1, over land) and 2.1 μm (band 7, over land and sea). In addition, effective radius retrievals are available using the channels at 1.6 μm (band 6) and 3.7 μm (band 20) together with band 1. Note that band 6 on the Aqua satellite suffers from a stripe-problem (Meirink et al., 2013). In this study MODIS collection 5.1 is used for the retrieved cloud optical depth and effective radius.

The ground remote sensing instruments of the Leipzig Aerosol and Cloud Remote Observations System (LACROS) comprise a 35-GHz MIRA-35 cloud radar, a HATPRO (Humidity And Temperature PROfiler) microwave radiometer, and a CHM15X ceilometer, which are used also for field campaigns. All instruments are operated in a vertically pointing mode. The raw measurements are processed with the Cloudnet algorithm package (Illingworth et al., 2007). The output data is available in an unified temporal resolution of 30 s and a vertical grid of 30 m. Cloudnet uses further information from a NWP model (here: COSMO-DE). In this study we use the attenuation-corrected radar reflectivity from the cloud radar, together with its error estimate, the liquid water path obtained from the microwave radiometer, as well as the cloud base and top height retrieved from ceilometer and cloud radar, respectively. The vertical Doppler velocity from the cloud radar is also utilized. Furthermore Cloudnet provides a target classification applying a series of tests to discriminate cloud phase, drizzle or rain, and aerosols or insects.

3.2 Cases

For this study, we focus on four ideal cases to gain a better understanding of the microphysical processes within the cloud by ruling out side-effects accompanying complicated cloud scenes such as multi-layer clouds as well as possible. We consider single-layer cloud systems which are entirely liquid and non-drizzling as ideal. We chose cases in a way that cloud layers are well-observed by all ground-based instruments and by MODIS and SEVIRI. In this study, we present, selected from the LACROS observationsm, two temporally rather homogeneous cases (27 October 2011 observed at Leipzig, and 21 April observed at Krauthausen), and two more inhomogeneous cases (1 June 2012, 27 September 2012, both observed at Leipzig). In the following the terms homogeneous and inhomogeneous clouds always refer to the temporal homogeneity unless stated otherwise. For the ± 15 surrounding SEVIRI pixels of the ground observations, we calculate the spatial inhomogeneity parameter following Cahalan et al. (1994), which can be interpreted also in terms of temporal inhomogeneity (χ) if the frozen turbulence hypothesis is applied:

$$\chi = \frac{\exp(\overline{\ln \tau})}{\overline{\tau}} \quad (15)$$

A short overview of the cloud layer characteristics is given in Table 2. The cloud boundaries are shown along with the cloud radar reflectivity profile in Fig. 1. Although we do not focus on the satellite cloud tops in this study we included these in Fig. 1. While for some time periods a good agreement can be seen, also periods with large discrepancies are found. Differences may result from semitransparent cirrus cloud layers (21 April 2013), inversion layers (27 October 2011) or broken cloud conditions (1 June 2012 and 27 September 2012). In the following we sum up the synoptic conditions for each case.

A high pressure system dominates the synoptic weather pattern on 27 October 2011 (Fig. 1a). The temperature at the 850 hPa pressure level over Leipzig is around 5 °C. Therefore the stratocumulus cloud layer that is observed between 10:30 and 13:00 UTC consists entirely of water droplets. Its geometrical depth increases in the beginning of the observation period. The Cloudnet classification indicates a cloud deck even before (not shown), although the radar is not sensitive enough to detect the thin cloud layer between 10:00 and 10:30 UTC.

The weather pattern on 21 April 2013 (Fig. 1b) is quite similar compared to the first case with the high pressure influence being stronger. The temperatures at the 850 hPa pressure level are slightly positive. During the whole observation period at Krauthausen a closed cloud deck is visible. The ground-based observation of cloud top height shows only small variability, while the cloud base is more inhomogeneous during the beginning of the observation period. A thin overlying cirrus cloud deck can be observed around 10:00 UTC and between 11:00 - 12:00 UTC.

An upper-level ridge covers Central Europe on 1 June 2012 (Fig. 1c), but the area around Leipzig is also influenced by a surface low. Temperatures at 850 hPa lie around 10 °C. The stratocumulus cloud deck with the cloud tops slightly below 2000 m between 12:00 and 16:00 UTC is broken with some cloudy periods in the early afternoon that are not well detected by the cloud radar.

The weather pattern for the 27 September 2012 (Fig. 1d) shows Leipzig directly in front of a well pronounced trough. Temperatures at 850 hPa lie again around 10 °C and the cloud types vary between stratocumulus and shallow cumulus. The cloud base height increases throughout the day. After 16:00 UTC also some precipitation can be observed for a short time.

4 Results

The following investigation is built on the observations from ground (cloud base height from ceilometer, cloud top height and Z from cloud radar, Q_L from the microwave radiometer) and from passive satellites (τ, r_e).

We will first focus on ground-based retrievals and evaluate the adiabatic factor, followed by a comparison of ground-based N_d retrieval results using the FI and OE method. Aftewards the key quantities H, N_d, Q_L obtained from satellite observations of SEVIRI and MODIS will be evaluated against the respective ground-based observations. We calculate the cloud droplet number concentration and cloud geometrical depth from the passive satellite-derived τ, r_e, assuming in the first step $f_\mathrm{ad} = 1$ and in a second step the f_ad calculated from the ground-based observations.

4.1 Retrieval of cloud properties from ground

4.1.1 Cloud adiabatic factor

Entrainment of dry air leads to deviations from the linearly increasing q_L profile. The cloud adiabatic factor as calculated from Eq. (8) using Q_L from the microwave radiometer and $H_\mathrm{obs}^\mathrm{ground}$ can quantify such deviations.

The time series of the adiabatic factor calculated for the two homogeneous cases is shown in Fig. 2a,b. The adiabatic factor at 27 October 2011 lies in the range from 0.4 to 0.9. Short time periods with $f_\mathrm{ad} > 1$ occur. These "superadiabatic" points are likely to be artefacts, since the occurence of "superadiabatic" cloud profiles in nature is physically implausible. Such artefacts may easily arise due to uncertainties in Q_L and H_cloud for thin clouds. In contrast to the original Cloudnet code, our calculation of the adiabatic factor allows for values greater than one. Within Cloudnet "superadiabatic" profiles are avoided by increasing the cloud top height if the adiabatic integrated q_L is smaller than Q_L measured by the microwave radiometer. We omitted adiabatic factors with $f_\mathrm{ad} > 1.0$ since we believe that those are most likely affected by the measurement uncertainties. This can be seen when considering the uncertainties that influence the adiabatic factor. For example, consider a cloud with $Q_\mathrm{L} = 100\,\mathrm{g\,m^{-2}}$ and $H_\mathrm{obs}^\mathrm{ground} = 324$ m that is adiabatic ($f_\mathrm{ad} = 1$). The Q_L retrieval uncertainty (microwave radiometer instrument error + retrieval error) is approximately $20\,\mathrm{g\,m^{-2}}$ and the $H_\mathrm{obs}^\mathrm{ground}$ uncertainty of the ceilometer and the cloud radar is at least $\pm$ 60 m due to the vertical resolution. Accounting for the maximum uncertainty ($Q_\mathrm{L} = 120\,\mathrm{g\,m^{-2}}$, and $H_\mathrm{obs}^\mathrm{ground} = 64$ m) or ($Q_\mathrm{L} = 80\,\mathrm{g\,m^{-2}}$ and $H_\mathrm{obs}^\mathrm{ground} = 384$ m), the resulting adiabatic factor would be 1.81 or 0.57, respectively. This shows that with the current uncertainty limits of the ground-based observations the adiabatic factor is still prone to large uncertainties especially for geometrically thin clouds.

For cross-checking with an independent approach, we also calculate the adiabatic factor using the information of the radar reflectivity profile. We see in Fig. 3 that the mean adiabatic factor calculated from the radar profiles is generally a bit lower, and that the correlation for all four cases is quite good with 62 % to 95 %, and root mean square differences between 0.14 and 0.24. This difference is likely explained by uncertainties in $H_\mathrm{obs}^\mathrm{ground}$ and Q_L, but also in Z obtained from the cloud radar and the retrieved N_d. In the following we will use the adiabatic factor calculated from Q_L and $H_\mathrm{obs}^\mathrm{ground}$.

On 21 April 2013 we find values of the adiabatic factor f_ad between 0.2 and 0.6 before 09:00 UTC. The radar reflectivity measurements (Fig. 1b) reveal that the cloud base is more inhomogeneous during this time period than later on. After 09:00 UTC the adiabatic factor oscillates between 0.5 and 1.0. Overall, the adiabatic factor also found for the other homogeneous case agrees well with the range of values of $[0.3, 0.9]$ suggested by Boers et al. (2006).

For the two inhomogeneous cases, the variability of the adiabatic factor (Fig. 2c,d) is larger than for the homogeneous cases considered before (Table 3), but the range of values is similar. This shows that independent from cloud homogeneity the majority of clouds seems to be sub-adiabatic.

Figure 4 reveals a tendency that geometrically thicker clouds are less adiabatic, while mainly the thin clouds ($H_{\mathrm{obs}}^{\mathrm{ground}} < 400\,\mathrm{m}$) are responsible for the "superadiabatic" cloud profiles. This supports the findings of Min et al. (2012), who observed the tendency that thicker clouds are less adiabatic in the Southeast Pacific. The investigation of thin clouds remains challenging. We therefore neglect cloud profiles with $f_{\mathrm{ad}} > 1$ in the following.

Schmidt et al. (2014a) used observations of two cases with homogeneous stratocumulus clouds over Leipzig, Germany, and found that in case of occurence of updrafts in clouds, the q_{L} profile is more adiabatic. To investigate if such a behaviour also occurs for our cases we apply the cloud radar Doppler velocity. The average vertical velocity of each cloud profile is found at -0.1 ms^{-1} with the majority of points in the range [-1,1] ms^{-1}. Considering this vertical velocity as function of cloud adiabacity we find a large spread, which makes it difficult to detect a clear dependence of cloud adiabacitity on updraft speed. However if we calculate the median adiabatic factor for the updraft and downdraft regimes individually, we find for each of our cases that clouds are slightly more adiabatic in the updraft regime (Table 3). This behaviour is expected from adiabaticity and also supported by the findings of Schmidt et al. (2014a). They report that this effect is strongest at the cloud base and blurs when the data points are averaged over the whole cloud profile.

4.1.2 Cloud droplet number concentration from radar-radiometer retrievals

N_{d} is used as the main parameter in many investigations of the first indirect aerosol effect. Advances have been made over the last two decades to apply retrievals for N_{d} combining ground-based cloud radar and microwave radiometer. We applied such a method following Fox and Illingworth (1997) (hereafter: FI, see Sect. 2.2.1). Furthermore we compare those results with the newly developed Optimal Estimation approach (see Sect. 2.2.2).

Contrasting the N_{d} from OE with the FI method, we find that the absolute mean difference of $N_{\mathrm{d}}^{\mathrm{OE}}$ and $N_{\mathrm{d}}^{\mathrm{FI}}$ considering all cases is $164\,\mathrm{cm}^{-3}$ (19 %). Overall, the FI method tends to yield lower values than the OE method, even though some outliers with unreasonably large values can be found ($N_{\mathrm{d}}^{\mathrm{OE}} > 2000\,\mathrm{cm}^{-3}$). In contrast to the FI method the OE method is also able to give information about the remaining uncertainty by considering measurement uncertainties as well as the uncertainty of the background state. With a quite large background uncertainty assumed to be $300\,\mathrm{cm}^{-3}$, we can see that the information (measurement and uncertainties) from the ground observation is able to reduce the final analysis error for N_{d}, but more constraints are required to obtain N_{d} with even higher accuracy. This would be desirable to better evaluate satellite observations.

4.2 Comparison of cloud properties from satellite and ground

Cloud microphysical retrievals that are based on either satellite or ground-based remote sensing both have their advantages and shortcomings. However, when the results of both approaches are in agreement, it is likely that the corresponding cloud layers are well suited for the investigation of key factors determining the first indirect effect.

By comparing ground-based and satellite observations, we have to consider the different spatial and temporal resolution, different error sources of the instruments as well as the different viewing zenith angle on the cloudy scene. For SEVIRI we have to consider a parallax shift at higher latitudes. The satellite viewing zenith angle for Leipzig is 58.8 °. Within this study the average cloud top height is between 1 km and 3 km (see Table 2). This would result in a horizontal displacement of max. 5 km. Considering the spatial resolution of SEVIRI over Central Europe of 4 km x 6 km, we decided to neglect the parallax correction for our study. To address the uncertainty of the satellite observations from SEVIRI and also MODIS we calculated the standard deviation of the surrounding pixels. For SEVIRI ± 1 pixel around the central pixel is added, resulting in a field of 9 satellite pixels. To cover a comparable area for MODIS, we add ± 9 pixel around the central pixel. For the comparison of the time series obtained from space and ground we applied data averaging only if mentioned. As pointed out in the following discussion for inhomogeneous scenes, omitting temporal averaging can lead to considerable differences of ground and satellite quantities.

4.2.1 Liquid water path

Considering the uncertainty of $20\,\mathrm{gm}^{-2}$ in Q_{L} for the ground-based microwave radiometer, the absolute mean difference between SEVIRI and the ground-based MWR is in good agreement. We find mean differences (relative mean difference) of $11\,\mathrm{gm}^{-2}$ (14%) for 21 April 2013, $16\,\mathrm{gm}^{-2}$ (28%) for 27 October 2011, $27\,\mathrm{gm}^{-2}$ (62%) for 1 June 2012 and $22\,gm^{-2}$ (42%) for 27 September 2012.

On 27 October 2011 we find larger differences in Q_{L} mainly after 12:00 UTC with up to $100\,\mathrm{gm}^{-2}$ (Fig. 5). Although rain might be a possible explanation for higher Q_{L} observed with the ground-based microwave radiometer, there are no are no signs for precipitation in both radar signal and satellite observations. The effective radius observed from satellite near cloud top lies clearly below the value of 14 μm which was suggested by Rosenfeld et al. (2012) as the threshold for drizzle/rain forming clouds. The maximum of the radar reflectivity in each profile did also not -20 dBZ, which is commonly taken as a drizzle threshold (Rémillard et al., 2013; Mace and Sassen, 2000). The observed difference might well be attributed to the satellite retrieved Q_L. For the same time period we also find disagreement in N_d from SEVIRI and ground and will discuss possible reasons in this context later.

For the inhomogeneous cases, the Q_L obtained from the ground-based microwave radiometer is highly variable. Especially the Cloudnet observations on 27 September 2012 show rapid changes of Q_L with peaks around $400\,\mathrm{gm}^{-2}$ and cloud-free periods. The SEVIRI temporal pattern is more smooth, because the satellite signal represents an average over different sub-pixel clouds within the field of view due to the lower spatial resolution.

4.2.2 Cloud geometrical depth

Contrasting $H_\mathrm{ad}^\mathrm{SEVIRI}$ with the $H_\mathrm{obs}^\mathrm{ground}$ (Fig. 6), we are able to investigate the same quantity obtained with two independent physical retrieval approaches. The correlation coefficient is 0.47 for 21 April 2013 after 09:00 UTC, 0.59 for 27 October 2011, 0.41 for 1 June 2012, and 0.12 for 27 September 2012. The correlation increases when temporally averaging is applied (Table 4). The improvement of correlation is not surprising when comparing averaged data as also pointed out in other studies (Deneke et al., 2009). However, a longer averaging period could remove the original variability of the data. The correlations for temporally averaged data are within the range of values that were obtained by Roebeling et al. (2008b), Min et al. (2012) and Painemal and Zuidema (2010). Roebeling et al. (2008b) found correlations of 0.71 between SEVIRI and Cloudnet for a homogeneous stratocumulus cloud layer. Min et al. (2012) found correlations of 0.62 between in-situ and MODIS retrieved H, and could show a better agreement of H when the adiabatic factor is explicitely calculated and considered. Painemal and Zuidema (2010) found correlations of 0.54 (0.7 for $H < 400\,\mathrm{m}$ with cloud fraction$> 90\,\%$) comparing radiosonde-derived cloud geometrical depth to respective MODIS observations. In their study Painemal and Zuidema (2010) reported that satellite values were higher compared to the ground-based ones. The reason for this can potentially be explained by a bias of MODIS-retrieved r_e but also in the choice of the adiabatic factor in the retrieval of H (Eq. 6). Satellite derived H increases if we choose $f_{ad} < 1$ instead of $f_{ad} = 1$.

If the adiabatic factor obtained from ground is applied to Eq. 6 instead of $f_{ad} = 1$, we find that the mean difference (relative mean difference) for the two homogeneous cases reduces from 87 m (31 %) to 45 m (16 %) for 27 October 2011, and from 87 m (23 %) to 14 m (4 %) for 21 April 2013. The same holds true for the inhomogeneous case at 27 September 2012 with a reduction from 149 m (47 %) to 90 m (29 %), but not for 1 June 2012 where the mean difference increases from 86 m (24 %) to 216 m (60 %).

For the cases investigated here, we saw a better agreement in H for available MODIS retrievals compared to SEVIRI if $f_\mathrm{ad} = 1$ is choosen. Indeed, clouds are actually subadiabatic while the retrieval assumes adiabatic clouds. This could counteract a high bias in MODIS r_e that is reported in previous studies (Marshak et al., 2006). For the four cases considered in this study, the number of collocated observations with MODIS is not sufficient in order to determine which effect is predominant for the bias. Therefore a larger dataset would be desirable for a more in-depth investigation.

4.2.3 Cloud droplet number concentration

The retrieval of N_d from passive satellite observations relies on the (sub-)adiabatic cloud model. In the following we contrast N_d retrieved from ground with the OE method and the adiabatic ($f_{ad} = 1$) retrieved values from MODIS and SEVIRI. The retrieved N_d are shown in Fig. 7. At 21 April 2013 the values agree within the uncertainty range with a mean difference (relative mean difference) of $29\,\mathrm{cm}^{-3}$ (10%) between SEVIRI and OE retrievals for the whole time period. For 27 September 2012 and 1 June 2012 we find mean differences (relative mean differences) of $23\,\mathrm{cm}^{-3}$(7%) and $103\,\mathrm{cm}^{-3}$ (43 %), respectively. At 27 October 2011 we find larger differences between SEVIRI and the ground-based N_d. At the beginning of the observation period (before 10:30 UTC) the $N_\mathrm{d}^\mathrm{SEVIRI}$ values are much lower than the N_d^OE ones. After 10:30 UTC $N_\mathrm{d}^\mathrm{SEVIRI}$ shows twice as large values as N_d^OE, resulting in a mean difference of $488\,\mathrm{cm}^{-3}$ (154 %) for the whole day.

To find explanations for the large deviations found on 27 October 2011, we calculated optical depth and effective radius from N_d^OE and $H_\mathrm{obs}^\mathrm{ground}$, respectively, using the adiabatic model (Eq. (3) and Eq. (4)). By comparing these to the satellite-retrieved values we are able to attribute the observed differences mainly to differences in effective radius, for which SEVIRI gives lower values (Fig. 5c). Before 10:30 UTC the mean difference in the effective radius is 2.5 μm compared to 3.4 μm afterwards. Q_L differences (Fig. 5a) can be attributed mainly to optical depth differences (Fig. 5b), which follows the same temporal pattern. Comparing the two satellite observations of the same cloud scene in the area of around $\pm 100\,\mathrm{km}$ around Leipzig (not shown), we find spatial inhomogeneities of cloud microphysics that can not be resolved in the same way by SEVIRI as it is possible for MODIS. Furthermore SEVIRI has to deal with a large solar zenith angle ($> 60°$) under relative azimuth angles close to 180° around noon, for which Roebeling et al. (2006) pointed out the lower precision of the retrieval.

Another influencing factor is the difference of the effective radius retrieval due to the different channels used by MODIS (2.1 μm) and SEVIRI (1.6 μm) for the standard retrieval products. From MODIS, additional effective radius retrievals from channels at 1.6 μm and 3.7 μm are available. Theoretically, the 3.7-μm channel should represent the effective radius close to the cloud top for adiabatic clouds, while the 2.1-μm and 1.6-μm channels receive the main signal from deeper layers within the cloud. Cloud observations do not always show an increase of effective radius from channel 1.6 μm over 2.1 μm to 3.7 μm as is expected for plane-parallel, adiabatic clouds (Platnick, 2000; King et al., 2013). Comparing mean differences of effective radius from SEVIRI and each of the three available MODIS channels, we find the smallest difference in r_e considering the MODIS channel at 1.6 μm. The mean difference in this case is 0.86 μm. This is not surprising as both channels cover more or less the same wavelength range. The difference increases when MODIS channels 2.1 μm and 3.7 μm are used. Intercomparing the effective radii retrieved from the three MODIS channels results in slightly smaller differences. The difference of MODIS channels at 2.1 μm and at 1.6 μm is 0.68 μm, while the difference of the retrieval at MODIS channels at 2.1 μm and at 3.7 μm is 0.51 μm.

Due to the $N \propto r_e^{-2.5}$ relationship (see Eq. 5) even small differences of effective radius result in large uncertainties of N_d. Explicitely considering this error propagation, we find for 27 October 2011 at 11:45 UTC that the observed difference in effective radius of 1.33 μm between MODIS and SEVIRI results in an uncertainty of 306 cm^{-3}. The uncertainty due to differences in effective radius of 0.34 μm between MODIS channels 2.1 μm and 1.6 μm is 57 cm^{-3}.

The importance of r_e for the retrieval of N_d from passive satellite imagers has already been pointed out by previuos studies. Those which were mainly based on MODIS (Painemal and Zuidema, 2010, 2011; Ahmad et al., 2013; Zeng et al., 2014). Painemal and Zuidema (2010) report a high bias of MODIS-derived r_e, but also state that the choice of the other parameters in the retrieval (namely k, Γ_ad) is able to compensate for this effect so that still a good agreement between MODIS retrieved and in-situ values could be achieved. A high bias of r_e occurs for broken cloud conditions (Marshak et al., 2006). Zeng et al. (2014) also saw a good agreement for MODIS derived N_d (using $f_\mathrm{ad} = 0.8$) with CALIOP (Cloud-Aerosol Lidar with Orthogonal Polarization), although they found a high bias in r_e compared to POLDER (Polarization and Directionality of the Earth Reflectance). Ahmad et al. (2013) also points out the importance of the effective radius for the N_d retrieval. As mentioned before, for our study only few MODIS observation points are available, but we already see that discrepancies in r_e in comparison to SEVIRI are a major source of uncertainty for N_d.

Janssen et al. (2011) also state for satellite retrievals of N_d (and also H_ad) that f_ad and Γ_ad are the most important uncertainty factors. They estimated the uncertainty of k to be negligible (around 3%). By considering the whole seasonal variability of cloud base temperature, they obtained an error of 24% for the adiabatic lapse rate of liquid water mixing ratio ($\Gamma_\mathrm{ad}(T,p)$). In our study Γ_ad has a smaller contribution to those uncertainties due to the fact that we are using model data to gain more reliable information about cloud base temperature and pressure instead of considering one constant value like in e.g. Quaas et al. (2006). If we compare Γ_ad calculated from satellite cloud top temperature and pressure with the one calculated from cloud base values observed from gound we find an uncertainty of 15% considering all 4 cases. As we see some deviations in the cloud top height, we believe that this can be mainly attributed to wrong satellite estimates of cloud top temperature and pressure. Janssen et al. (2011) further assumed an uncertainty in the adiabatic factor of 0.3. This resulted in a numerically evaluated error of around 26% considering typical values of effective radius and optical depth. To highlight the importance of considering the actual adiabatic factor for the retrieval process, we calculated the optical depth (Eq. (3)) and effective radius (Eq. (4)) from the ground-based observations using N_d^OE and $H_\mathrm{obs}^\mathrm{ground}$ with adiabatic factor $f_\mathrm{ad} = 1$ or the ground-obtained adiabatic factor. Afterwards we compare it to the satellite-retrieved values obtained with the CPP algorithm. When the adiabatic factor is assumed constant of $f_\mathrm{ad} = 1$ the mean difference in optical depth is 9.95 on 21 April 2013. When the adiabatic factor obtained from the ground-based measurements is considered, this mean difference is drastically reduced to 2.90. The mean difference of effective radius is reduced from 1.15 μm to 0.12 μm.

Therefore, we aim to adjust $N_\mathrm{d}^\mathrm{SEVIRI}$ Eq. 5 for the homogeneous cases by setting the adiabatic factor to the value obtained from the ground-based observation. The results can be seen in Fig. 8. On 2013-04-21 the adjusted $N_\mathrm{d}^\mathrm{SEVIRI}$ is generally slightly lower due to the observed sub-adiabaticity. Only before 09:00 UTC the adjustments lead to a better comparison to ground-obtained values. This case still shows the smallest relative mean difference of SEVIRI and ground-retrieved N_d with 15 %. For 27 October 2011 the retrieved $N_\mathrm{d}^\mathrm{SEVIRI}$ is also generally reduced, diminishing also the mean difference to the ground-retrieved values in this case (relative mean difference is reduced from 154 % to 114 %). The reason that including the adiabatic factor does not always lead to a better agreement can likely be attributed to the uncertainties of ground observations (discussed in Sect. 4.1.1). Although we were not able to see always an improvement in agreement of N_d by considering the ground-based calculated f_ad, Min et al. (2012) found a better agreement in N_d when considering it in their study. Since clouds are clearly sub-adiabatic in all our 4 cases independent of season, we believe that applying an adiabatic factor smaller than one is advantageous over considering adiabatic clouds in the retrieval.

For the inhomogeneous cases shown in Fig. 7c,d, a high temporal variability in N_d^OE can be seen. N_d^MODIS and the N_d^OE agree well within the uncertainty range. For the comparison of $N_\mathrm{d}^\mathrm{SEVIRI}$ and N_d^OE we find good agreement in the beginning and end of the observation period at 1 June 2012, when the clouds are more homogeneous.

The underestimation of $N_{\mathrm{d}}^{\mathrm{SEVIRI}}$ comprared to $N_{\mathrm{d}}^{\mathrm{OE}}$ can likely be attributed to broken-cloud effects on the SEVIRI retrieval. For broken clouds within the SEVIRI pixel the satellite receives a combined signal from the clouds but also from the surface. The same explanation can also be applied to the second inhomogeneous case (27 September 2012). It remains open to which extent the subpixel surface contamination leads to a bias in the retrieved cloud parameters especially for inhomogeneous cloud scenes when the brightness temperature actually does not represent the cloud radiative temperature.

While some of the differences between satellite- and ground-based retrievals of N_{d} can be attributed to the invalidity of the adiabatic assumption and coarse spatial resolution of the satellites, it has to be mentioned that the ground-based retrieval strongly relies on the accuracy of the radar reflectivity and therefore also on the radar calibration and attenuation corrections for atmospheric gases and liquid water that are made within the Cloudnet algorithm. Löhnert et al. (2003) points out the strong influence of drizzle on the cloud reflectivity. Errors of 30-60 % have to be anticipated for q_{L} profile retrievals. Those retrieval approaches are based on very similar principles as our OE method (Löhnert et al., 2001). In our study we filtered out drizzling profiles as well as possible, but the radar reflectivity still remains very sensitive to few larger droplets in a volume, which can not totally be ruled out. Therefore also the correct radar calibration is an issue.

5 Summary and Conclusions

To investigate the accuracy of satellite-based estimates of aerosol indirect effects, we have studied the validity of the (sub-)adiabatic cloud model as a conceptional tool commonly applied in previous studies (e.g. Bennartz, 2007; Schueller et al., 2003). The (sub-)adiabatic cloud model allows indirectly to estimate cloud geometrical depth (H_{cloud}) and cloud droplet number concentration (N_{d}) from passive satellite observations.

As reference, we used a combination of ground-based active and passive remote sensing instruments with high temporal and vertical resolution to provide detailed information of the cloud vertical structure. We could, however, demonstrate that such retrievals also have considerable uncertainties.

Considering the number of uncertainties for both the satellite and ground perspective, and those originating from the issue of representativity of the two perspectives, our comparison showed that the temporal evolution of cloud micro- and macrophysical quantities is captured surprisingly well for some cases. We discussed the large uncertainties that may occur depending on the observed scene and observation geometry.

The cloud geometrical depth can be obtained with ground-based remote sensing directly from ceilometer cloud base and radar cloud top heights. The mean difference of SEVIRI and ground-based cloud geometrical depth is lowest for the two presented homogeneous cases when the ground-based adiabatic factor is considered with values down to 14 m (4 %). Overall we found sub-adiabatic cloud layers. The adiabatic factor varied in time and attained values similar to those reported by Boers et al. (2006). For 3 out of 4 cases we obtained similar median values around 0.65 ± 0.2 at different seasons. Although larger datasets are required to draw robust conclusions about a typical adiabtic factor, this value could be a first guess for homogeneous stratocumulus clouds as they occur over Central Europe. For thin clouds the uncertainties remains large due to the high relative uncertainties of liquid water path and cloud geometrical depth. This also leads to superadiabatic artefacts in the retrieval. With increasing geometrical depth, the clouds become less adiabatic. We also found that clouds are slightly more adiabatic when the cloud profile is dominated by positive vertical velocity (updrafts). Although a larger dataset would be desirable to draw more robust conclusions, our results support those from Schmidt et al. (2014a) and Schmidt et al. (2014b).

We developed an Optimal Estimation (OE) retrieval to estimate N_{d} from ground-based radar and microwave radiometer observations, which does not require the assumption of a linear increasing liquid water content profile. While the mean difference of N_{d} retrieved from SEVIRI and the ground-based OE was $29\,\mathrm{cm}^{-3}$ (10 %) for one of the two homogeneous cases, for the second one we saw a large bias of $488\,\mathrm{cm}^{-3}$ (154 %). In these the MODIS retrieval was closer to the ground-retrieved values. We were able to attribute this large bias mainly to an underestimation of the effective radius within the current SEVIRI retrieval. Even small differences in effective radius result in large uncertainties of cloud droplet number concentration due to the $N_{\mathrm{d}} \propto r_{\mathrm{e}}^{-2.5}$-relationship. Further research about the influence of observation geometry and spatial resolution effects on effective radius and optical depth differences between MODIS and SEVIRI is required. The OE approach to retrieve cloud droplet number concentration from ground could be further improved by including more independent observations, e.g. from solar radiation observations (e.g. Brückner et al., 2014), which are available at several ground-based supersites as for LACROS.

Indications have been detected throughout this study that assumptions about cloud subadiabacity may help to explain differences between satellite and ground-based retrievals. Therefore, satellite retrievals should take into account that liquid water clouds are mostly subadiabatic.

So far only four cases were analyzed, but given the network of Cloudnet/ACTRIS in Central Europe this offers the opportunity to investigate the climatology of the adiabatic factor and investigate its regional, seasonal or synoptical dependency. Using more data from a greater network would give statistically more robust insights.

Acknowledgements. The first author's work was funded by the Leibzig Graduate School on Radiation (LGS-CAR). We would like to thank the Cloudnet project (European Union Contract EVK2-2000-00611) for providing the ground-based cloud products, and the EUMETSAT SAFS for providing the SEVIRI cloud products, as well as the NASA's Earth-Sun System Division for providing MODIS cloud products. We further acknowledge collegues participating in the HOPE campaign of the HD(CP)^2 project in Jülich. We also thank our collegues Anja Hünerbein, Andreas Macke, Fabian Senf, Johannes Quaas and two anonymous reviewers for their helpful suggestions and comments.

References

Ackerman, A. S., Toon, O. B., Taylor, J. P., Johnson, D. W., Hobbs, P. V., and Ferek, R. J.: Effects of Aerosols on Cloud Albedo: Evaluation of Twomey's Parameterization of Cloud Susceptibility Using Measurements of Ship Tracks, Journal of the Atmospheric Sciences, 57, 2684–2695, doi:10.1175/1520-0469(2000)057<2684:EOAOCA>2.0.CO;2, http://dx.doi.org/10.1175/1520-0469(2000)057<2684:EOAOCA>2.0.CO;2, 2000.

Ahmad, I., Mielonen, T., Grosvenor, D., Portin, H., Arola, A., Mikkonen, S., Kühn, T., Leskinen, A., Juotsensaari, J., Komppula, M., Lehtinen, K., Laaksonen, A., and Romakkaniemi, S.: Long-term measurements of cloud droplet concentrations and aerosol-cloud interactions in continental boundary layer clouds, Tellus B, 65, http://www.tellusb.net/index.php/tellusb/article/view/20138, 2013.

Albrecht, B. A., Fairall, C. W., Thomson, D. W., White, A. B., Snider, J. B., and Schubert, W. H.: Surface-based remote sensing of the observed and the Adiabatic liquid water content of stratocumulus clouds, Geophys. Res. Lett., 17, 89–92, doi:10.1029/GL017i001p00089, http://dx.doi.org/10.1029/GL017i001p00089, 1990.

Bennartz, R.: Global assessment of marine boundary layer cloud droplet number concentration from satellite, Journal of Geophysical Research: Atmospheres, 112, n/a–n/a, doi:10.1029/2006JD007547, http://dx.doi.org/10.1029/2006JD007547, 2007.

Boers, R., Russchenberg, H., Erkelens, J., Venema, V., van Lammeren, A., Apituley, A., and Jongen, S.: Ground-Based Remote Sensing of Stratocumulus Properties during CLARA, 1996, Journal of Applied Meteorology, 39, 169–181, doi:10.1175/1520-0450(2000)039<0169:GBRSOS>2.0.CO;2, http://dx.doi.org/10.1175/1520-0450(2000)039<0169:GBRSOS>2.0.CO;2, 2000.

Boers, R., Acarreta, J. R., and Gras, J. L.: Satellite monitoring of the first indirect aerosol effect: Retrieval of the droplet concentration of water clouds, Journal of Geophysical Research: Atmospheres, 111, n/a–n/a, doi:10.1029/2005JD006838, http://dx.doi.org/10.1029/2005JD006838, 2006.

Boucher, O., Randall, D., Artaxo, P., Bretherton, C., Feingold, G., Forster, P., Kerminen, V., Kondo, Y., Liao, H., Lohmann, U., et al.: Clouds and aerosols, Climate Change, pp. 571–657, 2013.

Brenguier, J.-L., Pawlowska, H., Schüller, L., Preusker, R., Fischer, J., and Fouquart, Y.: Radiative Properties of Boundary Layer Clouds: Droplet Effective Radius versus Number Concentration, Journal of the Atmospheric Sciences, 57, 803–821, doi:10.1175/1520-0469(2000)057<0803:RPOBLC>2.0.CO;2, http://dx.doi.org/10.1175/1520-0469(2000)057<0803:RPOBLC>2.0.CO;2, 2000.

Brückner, M., Pospichal, B., Macke, A., and Wendisch, M.: A new multispectral cloud retrieval method for ship-based solar transmissivity measurements, Journal of Geophysical Research: Atmospheres, 119, 11,338–11,354, doi:10.1002/2014JD021775, http://dx.doi.org/10.1002/2014JD021775, 2014.

Cahalan, R. F., Ridgway, W., Wiscombe, W. J., Bell, T. L., and Snider, J. B.: The Albedo of Fractal Stratocumulus Clouds, Journal of the Atmospheric Sciences, 51, 2434–2455, doi:10.1175/1520-0469(1994)051<2434:TAOFSC>2.0.CO;2, http://dx.doi.org/10.1175/1520-0469(1994)051<2434:TAOFSC>2.0.CO;2, 1994.

Christensen, M. W. and Stephens, G. L.: Microphysical and macrophysical responses of marine stratocumulus polluted by underlying ships: Evidence of cloud deepening, Journal of Geophysical Research: Atmospheres, 116, n/a–n/a, doi:10.1029/2010JD014638, http://dx.doi.org/10.1029/2010JD014638, d03201, 2011.

Deneke, H., Knap, W., and Simmer, C.: Multiresolution analysis of the temporal variance and correlation of transmittance and reflectance of an atmospheric column, J. Geophys. Res., 114, D17 206, doi:10.1029/2008JD011680, http://dx.doi.org/10.1029/2008JD011680, 2009.

Derrien, M.: Algorithm theoretical basis document for cloud products (cma-pge01 v3.2, ct-pge02 v2.2, ctth-pge03 v2.2), Tech. rep., SAFNWC, 2012.

Dong, X., Ackerman, T. P., Clothiaux, E. E., Pilewskie, P., and Han, Y.: Microphysical and radiative properties of boundary layer stratiform clouds deduced from ground-based measurements, Journal of Geophysical Research: Atmospheres, 102, 23 829–23 843, doi:10.1029/97JD02119, http://dx.doi.org/10.1029/97JD02119, 1997.

Dong, X., Mace, G. G., Minnis, P., Smith, W. L., Poellot, M., Marchand, R. T., and Rapp, A. D.: Comparison of Stratus Cloud Properties Deduced from Surface, GOES, and Aircraft Data during the March 2000 ARM Cloud IOP, Journal of the Atmospheric Sciences, 59, 3265–3284, doi:10.1175/1520-0469(2002)059<3265:COSCPD>2.0.CO;2, http://dx.doi.org/10.1175/1520-0469(2002)059<3265:COSCPD>2.0.CO;2, 2002.

Fox, N. I. and Illingworth, A. J.: The Retrieval of Stratocumulus Cloud Properties by Ground-Based Cloud Radar, Journal of Applied Meteorology, 36, 485–492, doi:10.1175/1520-0450(1997)036<0485:TROSCP>2.0.CO;2, http://dx.doi.org/10.1175/1520-0450(1997)036<0485:TROSCP>2.0.CO;2, 1997.

Han, Q., Rossow, W. B., Chou, J., and Welch, R. M.: Global variation of column droplet concentration in low-level clouds, Geophysical Research Letters, 25, 1419–1422, doi:10.1029/98GL01095, http://dx.doi.org/10.1029/98GL01095, 1998.

Hansen, J. E. and Travis, L. D.: Light scattering in planetary atmospheres, Space Science Reviews, 16, 527–610, 1974.

Hewison, T.: 1D-VAR Retrieval of Temperature and Humidity Profiles From a Ground-Based Microwave Radiometer, Geoscience and Remote Sensing, IEEE Transactions on, 45, 2163–2168, doi:10.1109/TGRS.2007.898091, 2007.

Hünerbein, A., Deneke, H., Macke, A., Ebell, K., and Görsdorf, U.: Combining the Perspective of Satellite- and

Table 1. Overview of assumptions made for the (sub-)adiabatic cloud model applied to derive N_d and H in literature studies. The table lists the values chosen for Γ_{ad}, f_{ad} (*calc.* refers to explicitely calculated values from additional data) and k according to Eq. 8. The table is sorted by publication year starting with the oldest one.

study	location	instrument(s)	derived quantities	Γ_{ad} [$\cdot 10^{-3} gm^{-4}$]	f_{ad}	k
Szczozodrak 2001	Eastern Pacific + Southern Ocean	AVHRR	N_d	2.0	n.a.	n.a.
Schueller 2005	North Atlantic (marine)	MODIS	N_d, H	n.a.	n.a.	n.a.
Boers 2006	Southern Ocean (Cape Grim)	MODIS	N_d, H	const.	0.6	0.87
Quaas 2006, 2008	global	MODIS	N_d	1.9	1.0	0.8
Bennartz 2007	global	MODIS	N_d, H	T-dependent	0.8	0.8
Roebeling 2008	Europe (continental)	SEVIRI	N_d, H	Boers 2006	0.75	Boers 2006
George 2010	Southeast Pacific	MODIS	N_d	1.95	n.a.	n.a.
Painemal 2010	Southeast Pacific	MODIS	N_d, H	2.0	1.0	0.8
Janssen 2011	Finnland (continental)	MODIS	N_d, H	1.44	0.6	0.87
Painemal 2011	Southeast Pacific	MODIS	N_d	2.0	1.0	0.8
Min 2012	Southeast Pacific	MODIS	N_d, H	T-dependent	calc.	0.5-1.0
Ahmad 2013	Puijo (continental)	MODIS	N_d	n.a.	1.0	0.67
Painemal 2013	Southeast Pacific	MODIS, aircraft	N_d	$T_\mathrm{cbh}, p_\mathrm{cbh}$	0.9	0.88
Zeng 2014	global	A-Train	N_d, H	$T_\mathrm{cth}, p_\mathrm{cth}$	1.0	0.6438
this study	Germany (continental)	SEVIRI	N_d, H	$T_\mathrm{cbh}, p_\mathrm{cbh}$	calc.	0.8

Table 2. Cases used within this study ordered by date. The minimum cloud base height (CBHL) and the maximum cloud top height (CTHL) of the liquid cloud layer investigated are presented together with the temporal averaged inhomogeneity paramater (χ) as in Cahalan et al. (1994) calculated from the optical depth of the ± 15 surrounding SEVIRI pixels for each observation time. Furthermore the category for each case is listed.

Date	Time	Location	Min(CBHL) [m]	Max(CTHL) [m]	χ	category
27 Oct 2011	09:00–13:00 UTC	Leipzig	525 m	1056 m	0.87	homogeneous
1 Jun 2012	12:00–16:00 UTC	Leipzig	1336 m	2428 m	0.73	inhomogeneous
27 Sep 2012	08:00–18:00 UTC	Leipzig	775 m	2927 m	0.55	inhomogeneous
21 Apr 2013	08:00–12:00 UTC	Krauthausen	1485 m	2171 m	0.87	homogeneous

Table 3. Median and standard deviation of the adiabatic factor (calculated from Eq. 8) for individual and for all cases, respectively. Furthermore the median of the adiabatic factor, classified into updraft ($v \geq 0$) and downdraft ($v < 0$) regimes, and the fraction of subadiatic cloud profiles is shown. Adiabatic factors with $f_\mathrm{ad} > 1.0$ are omitted since we believe that those are likely affected by measurement uncertainties.

	all	21 Apr 2013	27 Sep 2012	27 Oct 2011	1 Jun 2012
median f_ad	0.63	0.64	0.64	0.68	0.44
stddev f_ad	0.22	0.18	0.23	0.15	0.24
median $f_\mathrm{ad}\,[v \geq 0]$	0.66	0.71	0.67	0.72	0.46
stddev $f_\mathrm{ad}\,[v \geq 0]$	0.22	0.18	0.21	0.15	0.25
median $f_\mathrm{ad}\,[v \leq 0]$	0.61	0.62	0.62	0.66	0.43
stddev $f_\mathrm{ad}\,[v \leq 0]$	0.22	0.18	0.24	0.14	0.24
fraction $f_\mathrm{ad} < 1$	0.84	0.99	0.70	0.97	0.85

Table 4. Correlation coefficient of H_obs from Cloudnet and H from SEVIRI with different averaging periods applied to both datasets.

Date	30 s unaveraged	10 min average	20 min average	30 min average
21 Apr 2013 (after 09:00 UTC)	0.47	0.68	0.66	0.78
27 Sep 2012	0.12	0.33	0.51	0.63
27 Oct 2011	0.59	0.68	0.68	0.76
1 Jun 2012	0.41	0.59	0.71	0.75

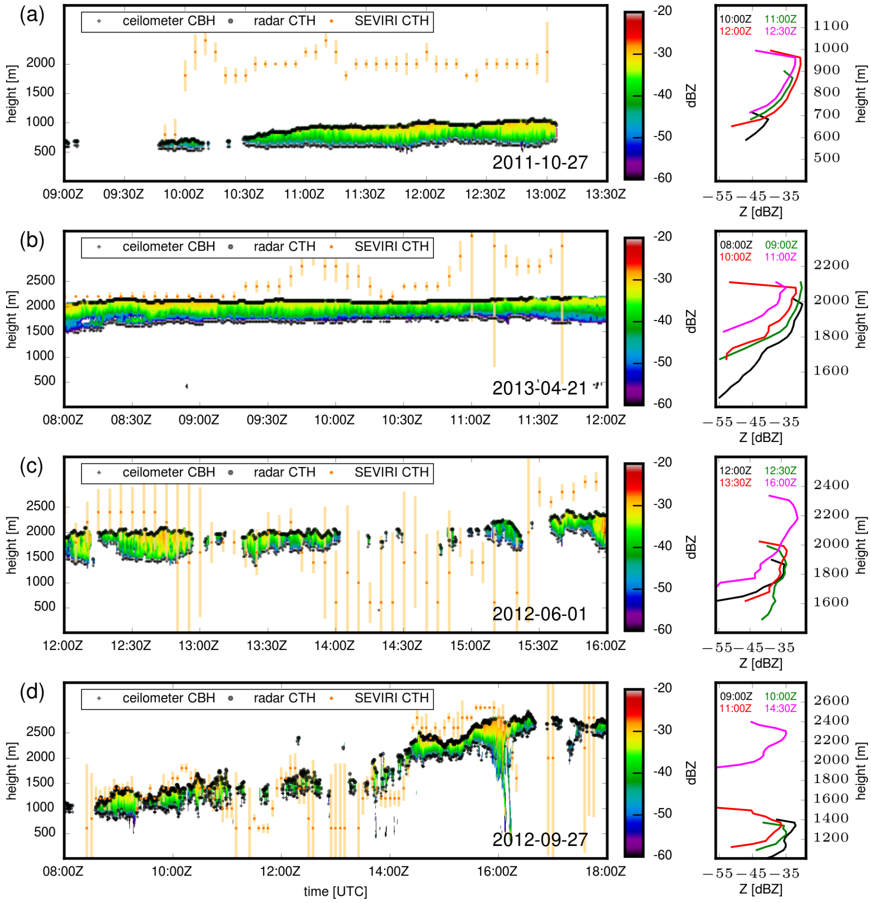

Figure 1. Time series of radar reflectivity (in dBZ) and cloud borders for the 4 cases listed in Table 2; (a) 27 October 2011, (b) 21 April 2013, (c) 1 June 2012, (d) 27 September 2012. Cloud borders are shown as detected by Cloudnet with black dots and by SEVIRI using NWCSAF in orange dots. Sample profiles of radar reflectivity are shown for each case at different times.

Ground-Based Observations to Analyze Cloud Frontal Systems, Journal of Applied Meteorology and Climatology, 53, 2538–2552, doi:10.1175/JAMC-D-13-0274.1, http://dx.doi.org/10.1175/JAMC-D-13-0274.1, 2014.

Illingworth, A., Hogan, R., O'connor, E., Bouniol, D., Delanoë, J., Pelon, J., Protat, A., Brooks, M., Gaussiat, N., Wilson, D., et al.: Cloudnet: Continuous evaluation of cloud profiles in seven operational models using ground-based observations, Bulletin of the American Meteorological Society, 88, 883–898, 2007.

Janssen, R. H. H., Ganzeveld, L. N., Kabat, P., Kulmala, M., Nieminen, T., and Roebeling, R. A.: Estimating seasonal variations in cloud droplet number concentration over the boreal forest from satellite observations, Atmospheric Chemistry and Physics, 11, 7701–7713, doi:10.5194/acp-11-7701-2011, http://www.atmos-chem-phys.net/11/7701/2011/, 2011.

King, N. J., Bower, K. N., Crosier, J., and Crawford, I.: Evaluating MODIS cloud retrievals with in situ observations from VOCALS-REx, Atmospheric Chemistry and Physics, 13, 191–209, doi:10.5194/acp-13-191-2013, http://www.atmos-chem-phys.net/13/191/2013/, 2013.

Lehmann, K., Siebert, H., and Shaw, R. A.: Homogeneous and Inhomogeneous Mixing in Cumulus Clouds: Dependence on Local Turbulence Structure, Journal of the Atmospheric Sciences, 66, 3641–3659, doi:10.1175/2009JAS3012.1, http://dx.doi.org/10.1175/2009JAS3012.1, 2009.

Löhnert, U., Crewell, S., Simmer, C., and Macke, A.: Profiling Cloud Liquid Water by Combining Active and Passive Microwave Measurements with Cloud Model Statistics, Journal of Atmospheric and Oceanic Technology, 18, 1354–1366, doi:10.1175/1520-0426(2001)018<1354:PCLWBC>2.0.CO;2, http://dx.doi.org/10.1175/1520-0426(2001)018<1354:PCLWBC>2.0.CO;2, 2001.

Löhnert, U., Feingold, G., Uttal, T., Frisch, A. S., and Shupe, M. D.: Analysis of two independent methods for retrieving liquid water profiles in spring and summer Arctic boundary clouds, Journal of Geophysical Research: Atmospheres, 108, n/a–n/a, doi:10.1029/2002JD002861, http://dx.doi.org/10.1029/2002JD002861, 2003.

Mace, G. G. and Sassen, K.: A constrained algorithm for retrieval of stratocumulus cloud properties using solar radiation, microwave radiometer, and millimeter cloud radar data,

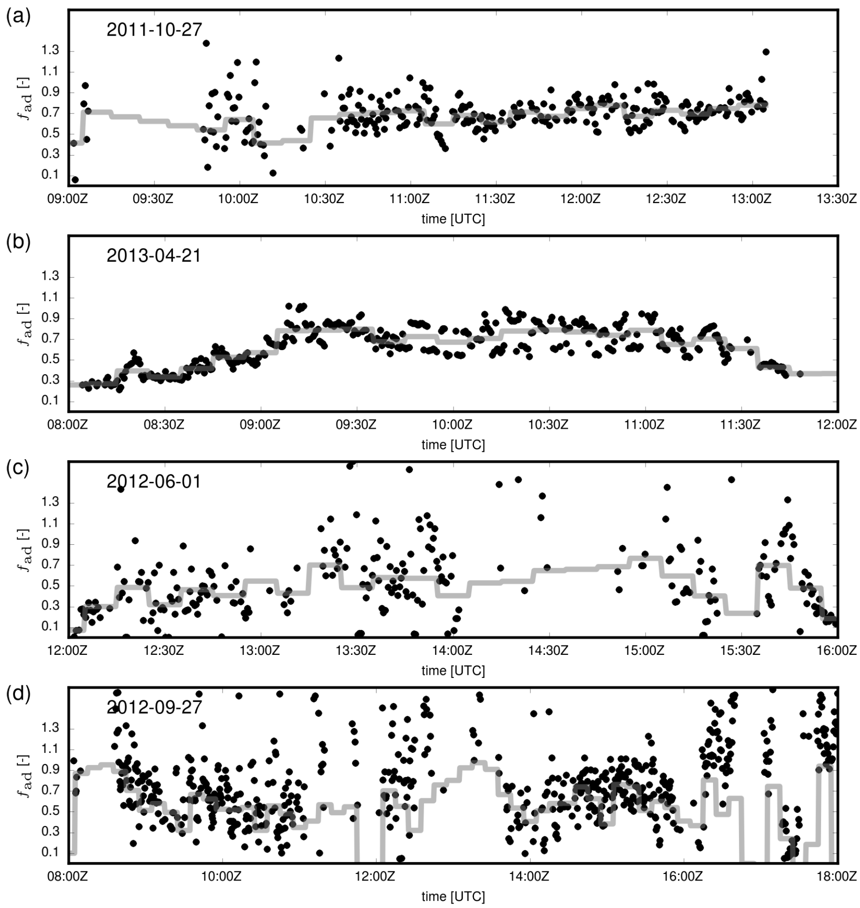

Figure 2. Adiabatic factor for all four cases. Black dots represent the adiabatic factor derived using ground-based geometrical depth and liquid water path from the microwave radiometer. The gray line represents the 10-min averaged and interpolated adiabatic factor neglecting superadiabatic values.

Journal of Geophysical Research: Atmospheres, 105, 29 099–29 108, doi:10.1029/2000JD900403, http://dx.doi.org/10.1029/2000JD900403, 2000.

Marshak, A., Platnick, S., Várnai, T., Wen, G., and Cahalan, R. F.: Impact of three-dimensional radiative effects on satellite retrievals of cloud droplet sizes, Journal of Geophysical Research: Atmospheres, 111, n/a–n/a, doi:10.1029/2005JD006686, http://dx.doi.org/10.1029/2005JD006686, d09207, 2006.

Martucci, G. and O'Dowd, C. D.: Ground-based retrieval of continental and marine warm cloud microphysics, Atmospheric Measurement Techniques, 4, 2749–2765, doi:10.5194/amt-4-2749-2011, http://www.atmos-meas-tech.net/4/2749/2011/, 2011.

Martucci, G., Milroy, C., and O'Dowd, C. D.: Detection of Cloud-Base Height Using Jenoptik CHM15K and Vaisala CL31 Ceilometers, Journal of Atmospheric and Oceanic Technology, 27, 305–318, doi:10.1175/2009JTECHA1326.1, http://dx.doi.org/10.1175/2009JTECHA1326.1, 2010.

Meirink, J. F., Roebeling, R. A., and Stammes, P.: Inter-calibration of polar imager solar channels using SEVIRI, Atmospheric Measurement Techniques, 6, 2495–2508, doi:10.5194/amt-6-2495-2013, http://www.atmos-meas-tech.net/6/2495/2013/, 2013.

Miles, N. L., Verlinde, J., and Clothiaux, E. E.: Cloud Droplet Size Distributions in Low-Level Stratiform Clouds, Journal of the Atmospheric Sciences, 57, 295–311, doi:10.1175/1520-0469(2000)057<0295:CDSDIL>2.0.CO;2, http://dx.doi.org/10.1175/1520-0469(2000)057<0295:CDSDIL>2.0.CO;2, 2000.

Min, Q., Joseph, E., Lin, Y., Min, L., Yin, B., Daum, P. H., Kleinman, L. I., Wang, J., and Lee, Y.-N.: Comparison of MODIS cloud microphysical properties with in-situ measurements over the Southeast Pacific, Atmospheric Chemistry and Physics, 12, 11 261–11 273, doi:10.5194/acp-12-11261-2012, http://www.atmos-chem-phys.net/12/11261/2012/, 2012.

Nakajima, T. and King, M. D.: Determination of the Optical Thickness and Effective Particle Radius of Clouds from Reflected Solar Radiation Measurements. Part I: Theory, Journal of the Atmospheric Sciences, 47, 1878–1893, doi:10.1175/1520-0469(1990)047<1878:DOTOTA>2.0.CO;2, http://dx.doi.org/10.1175/1520-0469(1990)047<1878:DOTOTA>2.0.CO;2, 1990.

Painemal, D. and Zuidema, P.: Microphysical variability in southeast Pacific Stratocumulus clouds: synoptic conditions and radiative response, Atmospheric Chemistry and Physics,

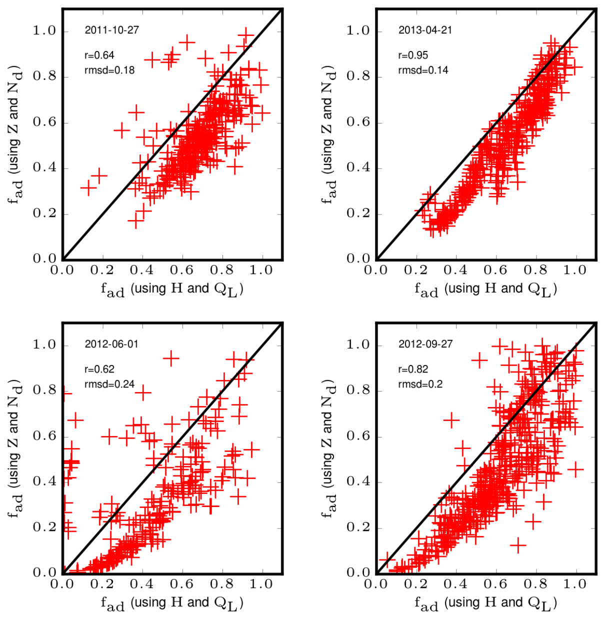

Figure 3. Adiabatic factor calculated from ground-based observations using H and Q_L (x-axis) and from Z and N_d (y-axis). Superadiabatic values are omitted. The graphs correspond to our four investigated cases (see Table 2).

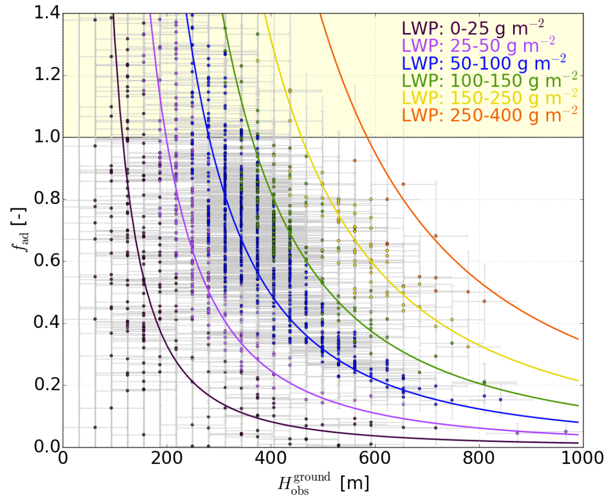

Figure 4. Adiabatic factor as a function of observed cloud geometrical depth (H_{obs}^{ground}) including data of all four cases. Colors indicate different liquid water path bins. The range with $f_{ad} > 1$ is shaded with light yellow. This superadiabatic range is neglected for the further study. The solid lines represent the relationship described in Eq. (8) for bin mean liquid water path and $\Gamma_{ad} = 1.9 \cdot 10^{-3}\mathrm{gm}^{-4}$.

10, 6255–6269, doi:10.5194/acp-10-6255-2010, http://www.atmos-chem-phys.net/10/6255/2010/, 2010.

Painemal, D. and Zuidema, P.: Assessment of MODIS cloud effective radius and optical thickness retrievals over the Southeast Pacific with VOCALS-REx in situ measurements, Journal of Geophysical Research: Atmospheres, 116, n/a–n/a, doi:10.1029/2011JD016155, http://dx.doi.org/10.1029/2011JD016155, 2011.

Placidi, S., Roebeling, R., Donovan, D., Boers, R., and Russchenberg, H.: Evaluation of Meteosat-8/SEVIRI retrieved cloud depth for water clouds using CloudNet sites, in: Joint 2007 EUMETSAT Meteorological Satellite Conference and the 15th Satellite Meteorology & Oceanography Conference of the American Meteorological Society, vol. P.50, pp. s8–s12, EUMETSET, Amsterdam, The Netherlands, 2007.

Platnick, S.: Vertical photon transport in cloud remote sensing problems, Journal of Geophysical Research: Atmospheres, 105, 22 919–22 935, doi:10.1029/2000JD900333, http://dx.doi.org/10.1029/2000JD900333, 2000.

Platnick, S., King, M. D., Ackerman, S. A., Menzel, W. P., Baum, B. A., Riédi, J. C., and Frey, R. A.: The MODIS cloud products: Algorithms and examples from Terra, Geoscience and Remote Sensing, IEEE Transactions on, 41, 459–473, 2003.

Quaas, J., Boucher, O., and Lohmann, U.: Constraining the total aerosol indirect effect in the LMDZ and ECHAM4 GCMs using MODIS satellite data, Atmospheric Chemistry and Physics, 6, 955, http://hal.archives-ouvertes.fr/hal-00328423, 2006.

Rémillard, J., Kollias, P., and Szyrmer, W.: Radar-radiometer retrievals of cloud number concentration and dispersion parameter in nondrizzling marine stratocumulus, Atmospheric Measurement Techniques, 6, 1817–1828, doi:10.5194/amt-6-1817-2013, http://www.atmos-meas-tech.net/6/1817/2013/, 2013.

Rodgers, C.: Inverse methods for atmospheric sounding, vol. 2 of Series on Atmospheric, Oceanic and Planetary Physics, 2000.

Roebeling, R., Placidi, S., Donovan, D., Russchenberg, H., and Feijt, A.: Validation of liquid cloud property retrievals from SEVIRI using ground-based observations, Geophysical Research Letters, 35, L05 814, 2008a.

Roebeling, R. A., Feijt, A. J., and Stammes, P.: Cloud property retrievals for climate monitoring: Implications of differences between Spinning Enhanced Visible and Infrared Imager (SEVIRI) on METEOSAT-8 and Advanced Very High Resolution Radiometer (AVHRR) on NOAA-17, Journal of Geophysical Research: Atmospheres, 111, n/a–n/a, doi:10.1029/2005JD006990, http://dx.doi.org/10.1029/2005JD006990, 2006.

Roebeling, R. A., Deneke, H. M., and Feijt, A. J.: Validation of Cloud Liquid Water Path Retrievals from SEVIRI Using One Year of CloudNET Observations, Journal of Applied Meteorology and Climatology, 47, 206–222, doi:10.1175/2007JAMC1661.1, http://dx.doi.org/10.1175/2007JAMC1661.1, 2008b.

Rosenfeld, D., Wang, H., and Rasch, P. J.: The roles of cloud drop effective radius and LWP in determining rain properties in marine stratocumulus, Geophysical Research Letters, 39, doi:10.1029/2012GL052028, http://dx.doi.org/10.1029/2012GL052028, 2012.

Saunders, R., Matricardi, M., and Brunel, P.: An improved fast radiative transfer model for assimilation of satellite radiance observations, Quarterly Journal of the Royal Meteorological Society, 125, 1407–1425, doi:10.1002/qj.1999.49712555615, http://dx.doi.org/10.1002/qj.1999.49712555615, 1999.

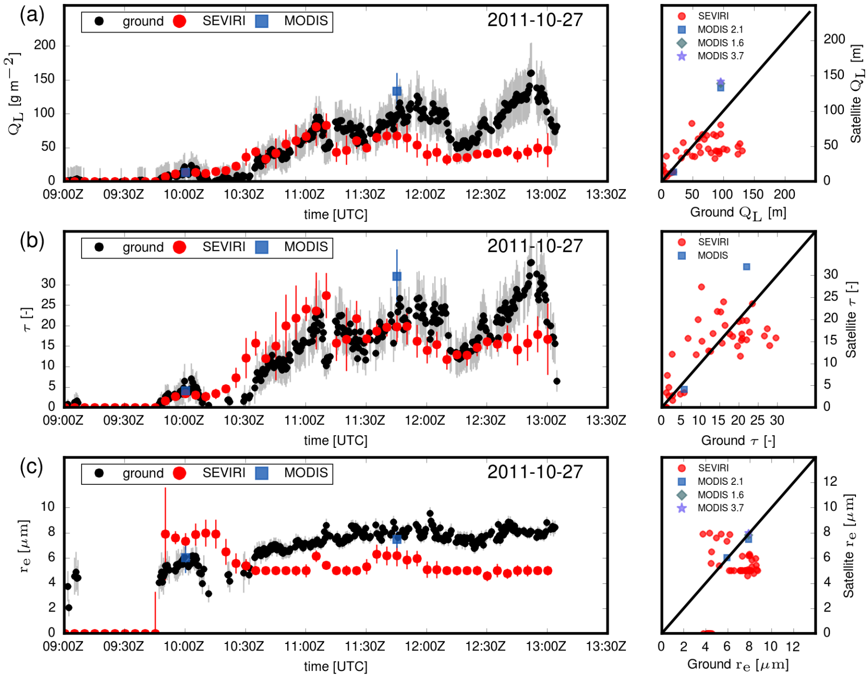

Figure 5. (a) Liquid water path for 27 October 2011 as obtained from the microwave radiometer (black dots), adiabatically from SEVIRI (red dots), and MODIS (green dots), respectively. For MODIS the effective radius obtained with three different channels is shown in the scatter plot with different symbols (square: 2.1 μm, diamond: 1.6 μm, star: 3.7 μm). (b) Time series of optical depth as obtained from SEVIRI (red), MODIS (green), and calculated from ground retrievals, respectively (black). (c) Time series of effective radius with the same colors. The variability of SEVIRI- and MODIS-derived values is given in terms of standard deviation of the surrounding area of ± 1 and ± 9 pixels, respectively.

Schmetz, J., Pili, P., Tjemkes, S., Just, D., Kerkmann, J., Rota, S., and Ratier, A.: An introduction to Meteosat Second Generation (MSG)., Bulletin of the American Meteorological Society, 83, 2002.

Schmidt, J., Ansmann, A., Bühl, J., Baars, H., Wandinger, U., Müller, D., and Malinka, A. V.: Dual-FOV Raman and Doppler lidar studies of aerosol-cloud interactions: Simultaneous profiling of aerosols, warm-cloud properties, and vertical wind, Journal of Geophysical Research: Atmospheres, 119, 5512–5527, doi:10.1002/2013JD020424, http://dx.doi.org/10.1002/2013JD020424, 2014a.

Schmidt, J., Ansmann, A., Bühl, J., and Wandinger, U.: Role of updrafts in aerosol-cloud interactions: lidar observations of layered warm clouds over central Europe, Atmospheric Chemistry and Physics Discussions, 14, 31 409–31 440, doi:10.5194/acpd-14-31409-2014, http://www.atmos-chem-phys-discuss.net/14/31409/2014/, 2014b.

Schueller, L., Brenguier, J.-L., and Pawlowska, H.: Retrieval of microphysical, geometrical, and radiative properties of marine stratocumulus from remote sensing, J. Geophys. Res., 108, 8631, doi:10.1029/2002JD002680, http://dx.doi.org/10.1029/2002JD002680, 2003.

Schulz, J., Albert, P., Behr, H.-D., Caprion, D., Deneke, H., Dewitte, S., Dürr, B., Fuchs, P., Gratzki, A., Hechler, P., Hollmann, R., Johnston, S., Karlsson, K.-G., Manninen, T., Müller, R., Reuter, M., Riihelä, A., Roebeling, R., Selbach, N., Tetzlaff, A., Thomas, W., Werscheck, M., Wolters, E., and Zelenka, A.: Operational climate monitoring from space: the EUMETSAT Satellite Application Facility on Climate Monitoring (CM-SAF), Atmospheric Chemistry and Physics, 9, 1687–1709, doi:10.5194/acp-9-1687-2009, http://www.atmos-chem-phys.net/9/1687/2009/, 2009.

Shupe, M. D.: A ground-based multisensor cloud phase classifier, Geophysical Research Letters, 34, n/a–n/a, doi:10.1029/2007GL031008, http://dx.doi.org/10.1029/2007GL031008, 2007.

Stephens, G. L., Vane, D. G., Boain, R. J., Mace, G. G., Sassen, K., Wang, Z., Illingworth, A. J., O'Connor, E. J., Rossow, W. B., Durden, S. L., Miller, S. D., Austin, R. T., Benedetti, A., Mitrescu, C., and CloudSat Science Team, T.: THE CLOUDSAT MISSION AND THE A-TRAIN, Bulletin of the American Meteorological Society, 83, 1771–1790, doi:10.1175/BAMS-83-12-1771, http://dx.doi.org/10.1175/BAMS-83-12-1771, 2002.

Turner, D. D., Vogelmann, A. M., Johnson, K., Miller, M., Austin, R. T., Barnard, J. C., Flynn, C., Long, C., McFarlane, S. A., Cady-Pereira, K., Clough, S. A., Chiu, J. C., Khaiyer, M. M., Liljegren, J., Lin, B., Minnis, P., Marshak, A., Matrosov, S. Y., Min, Q., O'Hirok, W., Wang, Z., and Wiscombe, W.: Thin Liquid Water Clouds: Their Importance and Our Challenge, Bulletin of the American Meteorological Society, 88, 177–190, doi:10.1175/BAMS-88-2-177, http://dx.doi.org/10.1175/BAMS-88-2-177, 2007.

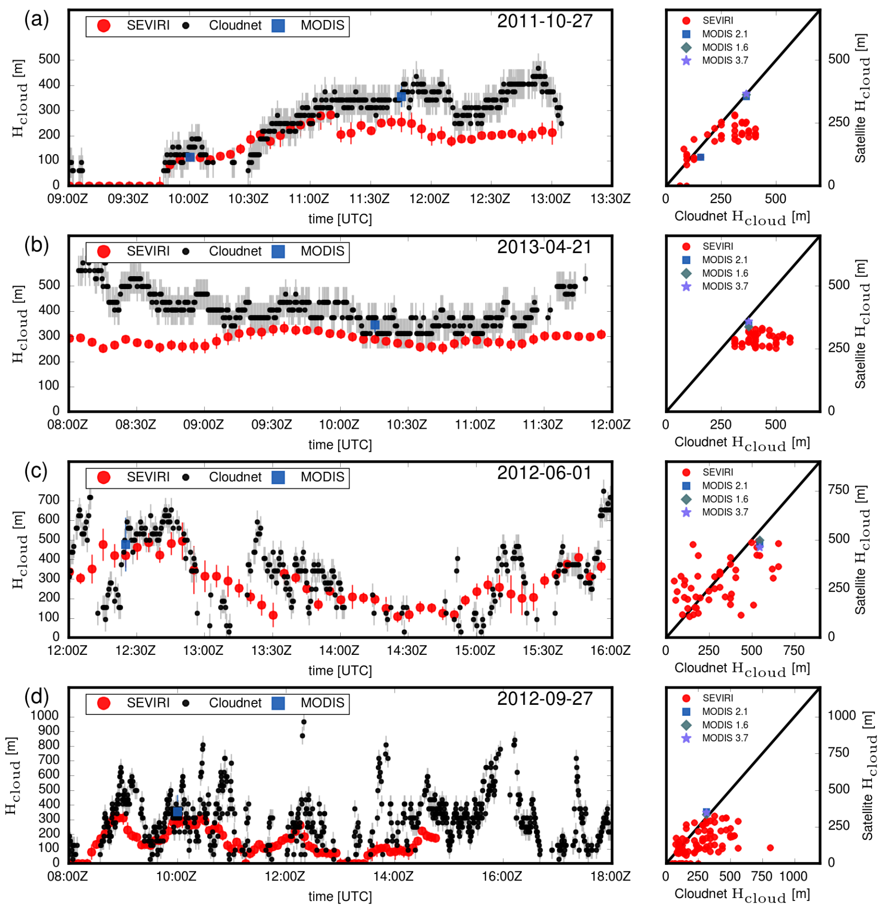

Figure 6. H_{cloud} for the four cases. Black dots represent the geometrical cloud depth observed from ground, red dots the SEVIRI adiabatically derived values, and green dots the MODIS adiabatically derived values. The uncertainties for the ground-based values are shown as shaded areas. The uncertainty estimates of MODIS and SEVIRI are represented in the same way as described in Fig. 5. In the scatter plots diamonds and stars represent the MODIS adiabatically derived values using available channels 1.6 μm and 3.7 μm, respectively.

Twomey, S.: Pollution and the planetary albedo, Atmospheric Environment (1967), 8, 1251 – 1256, doi:10.1016/0004-6981(74)90004-3, http://www.sciencedirect.com/science/article/pii/0004698174900043, 1974.

Winker, D. M., Vaughan, M. A., Omar, A., Hu, Y., Powell, K. A., Liu, Z., Hunt, W. H., and Young, S. A.: Overview of the CALIPSO Mission and CALIOP Data Processing Algorithms, Journal of Atmospheric and Oceanic Technology, 26, 2310–2323, doi:10.1175/2009JTECHA1281.1, http://dx.doi.org/10.1175/2009JTECHA1281.1, 2009.

Wood, R.: Relationships between optical depth, liquid water path, droplet concentration, and effective radius in adiabatic layer cloud, University of Washington, 3, 2006.

Zeng, S., Riedi, J., Trepte, C. R., Winker, D. M., and Hu, Y.-X.: Study of global cloud droplet number concentration with A-Train satellites, Atmospheric Chemistry and Physics, 14, 7125–7134, doi:10.5194/acp-14-7125-2014, http://www.atmos-chem-phys.net/14/7125/2014/, 2014.

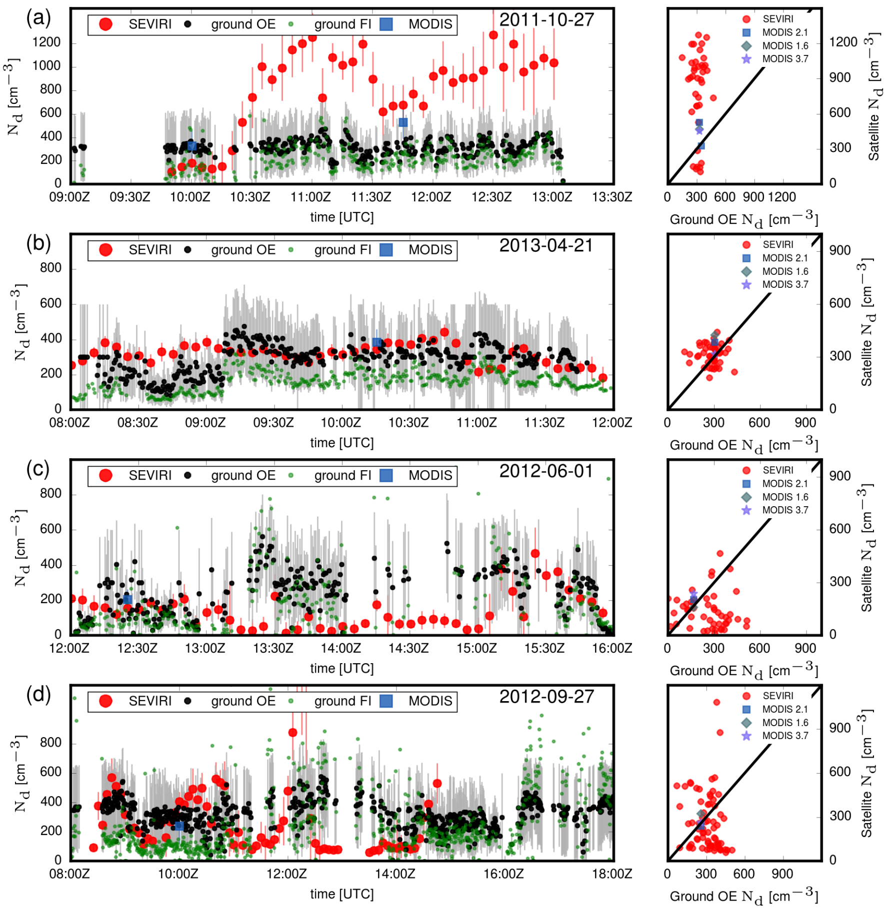

Figure 7. Time series of retrievals of the estimated cloud droplet number concentration. Black dots represent the OE method, using ground-based data (N_d^{OE}). The gray shaded area illustrates the uncertainty, calculated from the error covariance matrix of OE. Blue dots represent the retrieval with the FI method applied to ground site data (N_d^{FI}). Red dots represent the adiabatically derived values from SEVIRI (N_d^{SEVIRI}), while green dots those from MODIS (N_d^{MODIS}). Different MODIS channels used in the retrieval are denoted with the same symbols as in the figures before. Variability for SEVIRI and MODIS is given in terms of standard deviation of the surrounding area of ±1 and ±9 pixels, respectively.

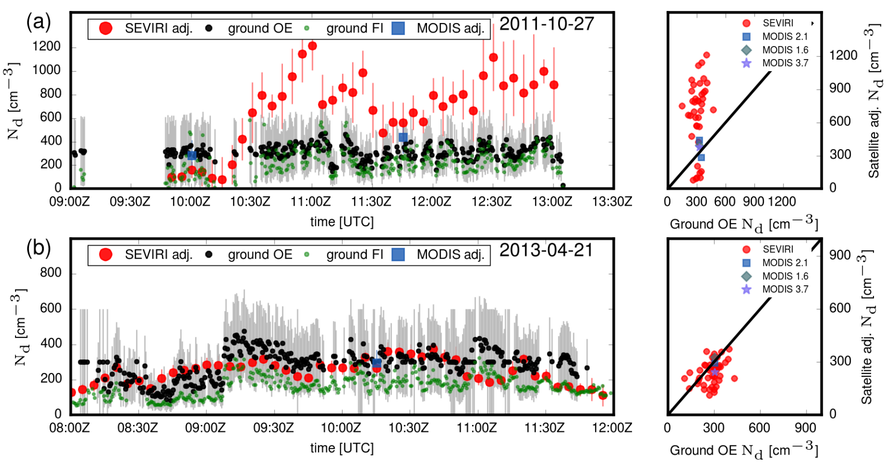

Figure 8. Adjusted cloud droplet number concentration from SEVIRI and MODIS applying f_{ad} from ground-based observations in Eq. 5 for the two homogeneous cases. Colors and symbols are the same as in Fig. 7.